Limitations of step profile models in describing the space-charge distribution near semiconductor surfaces

1997 J. Phys.: Condens. Matter 9 2903

(http://iopscience.iop.org/0953-8984/9/14/006)

J. Phys.: Condens. Matter **9** (1997) 2903–2914. Printed in the UK PII: S0953-8984(97)79026-X

Limitations of step profile models in describing the space-charge distribution near semiconductor surfaces

G R Bell†, C F McConville†§, C P A Mulcahy‡ and T S Jones‡

† Department of Physics, University of Warwick, Coventry CV4 7AL, UK

‡ Department of Chemistry, Imperial College of Science, Technology and Medicine, London SW7 2AY, UK

Received 29 October 1996

Abstract. High-resolution electron energy-loss (HREEL) spectra have been analysed using local dielectric theory in a study of the depletion layer formed at the InSb(100) surface. Two-, three- and four-layer models were used to simulate a series of low-incidence-energy HREEL spectra (1.25–10 eV). An abrupt charge profile (the two-layer model) provided good agreement with experimental data when spatial dispersion and wavevector-dependent plasmon damping were included in the local dielectric model. This was in spite of the fact that the two-layer model does not accurately reflect the charge distribution, which was calculated using the modified Thomas–Fermi approximation (MTFA). Smoothing of the step profile by the inclusion of an intermediate layer (the three-layer model) introduced 'plasmaron' modes, unless the plasma damping in the middle layer was set to a very high level. These modes were not observed experimentally, indicating that the abrupt charge profile in fact produced more accurate simulations. A four-layer model more closely approximating the calculated charge profile produced superior fits to the experimental spectra, but only when the plasma damping in each layer was carefully controlled. The limitations of step profile approximations and the local dielectric theory approach in describing regions of highly non-uniform charge density are discussed. In particular, the spatial and wavevector dependence of the plasmon damping is considered.

1. Introduction

High-resolution electron energy-loss spectroscopy (HREELS) is a versatile technique for studying the electronic properties and charge distribution in the near-surface region of III–V semiconductor materials [1–8]. Measurements of the surface and interfacial plasmon modes, and the degree of coupling to the optical phonon modes, provide information about important physical parameters such as band bending, surface state density, carrier concentration and electron mobility. These plasmon modes are also of fundamental interest as excitations of an inhomogeneous electron gas. Extraction of the parameters mentioned above requires experimental measurements of both the energy and intensity of these excitations at different incident electron beam energies, and simulation of the spectra using the semi-classical dielectric theory of HREELS [9, 10]. These simulations require detailed modelling of the near-surface region of the material.

The majority of previous HREELS studies on III–V semiconductors have been concerned with the formation of depletion layers at GaAs and InSb surfaces. The (110)

§ Tel.: +44 1203 524 236; fax: +44 1203 692 016; e-mail: C.F.McConville@warwick.ac.uk

0953-8984/97/142903+12$19.50

surface of GaAs has been the most extensively investigated with band bending introduced by the adsorption of hydrogen onto the cleaved surface [1, 6]. A two-layer model, involving a carrier-free layer on top of the bulk, has generally been found to be sufficient for modelling the experimental data and studying the effect of depletion layers on the plasmon and phonon modes. Depletion layers have also been studied on the (100) surface of GaAs [3] and InSb [11]. It is well known that the structural and electronic properties of the (100) surface are particularly sensitive to surface treatment. The preparation of clean surfaces is therefore more difficult and generally involves either desorption of a protective As (or Sb) capping layer following growth by molecular beam epitaxy (MBE) [3, 4, 12, 13], or cycles of low-energy ion bombardment and annealing [11, 14, 15].

In the case of InSb surfaces, early applications of semi-classical local dielectric theory were of limited success in simulating HREEL spectra. For InSb(110), Ritz and Lüth [2] modelled their data using a carrier-free depletion layer. Although this was successful in interpreting the variation in the plasmon intensity with incident electron beam energy, it did not reproduce the corresponding changes in the plasmon energy. A different theoretical approach was adopted by Inaoka *et al* [16], which involved a semi-classical infinite-barrier model and the random-phase approximation. Although neglecting any depletion layer, they showed that it was important to consider the non-parabolic nature of the conduction band and spatial dispersion of the plasmon excitation. More recently, we have shown that it is possible to get very good agreement between theory and experiment when HREELS data for degenerate InSb(100) are analysed using a two-layer model incorporating spatial dispersion and non-parabolicity [11]. Furthermore, this model accurately reflects the observed changes in the behaviour of the plasmon excitation at different substrate temperatures.

The adequacy of the abrupt two-layer model in describing the near-surface region of these materials is generally dependent on the magnitude of the Thomas–Fermi or Debye screening length relative to the thickness of the depletion layer. In this paper, we present a detailed analysis of HREEL spectra recorded from InSb(100) at high resolution and low incident electron energies (<10 eV). Good correlation is obtained between the experimental and theoretical spectra over the entire electron energy range, and surprisingly this is achieved using the simple two-layer model despite the model depletion layer thickness being approximately equal to the Thomas–Fermi screening length ($L_{TF} = 85$ Å). We compare both three- and four-layer models with the abrupt model and show that they require careful adjustment of the plasma damping coefficients to produce good fits to the experimental data. Without such adjustments, these models introduce plasmon–phonon coupling which is not observed experimentally. The four-layer model, based on a calculated charge distribution rather than on fitting procedures, produces the best fits with only the plasma damping coefficients as adjustable parameters. The ability of a multiple-step profile model to describe a highly inhomogeneous charge distribution is discussed, in particular with regard to the spatial dependence of the plasmon damping.

2. Experimental details

The experiments were carried out in an ultra-high-vacuum chamber (base pressure $\sim 2 \times 10^{-10}$ mbar) equipped with low-energy electron diffraction (LEED), Auger electron spectroscopy (AES) and HREELS. The HREEL spectrometer (HIB 1000) consists of a double-pass cylindrical monochromator and analyser assembly, with the analyser fixed and the monochromator rotatable [17]. The n-type (Si-doped, $n \sim 5 \times 10^{17}$ cm^{-3}) InSb(100) substrates were cleaned *in situ* by cycles of low-energy-argon-ion bombardment at grazing incidence (800 eV, 3 μA sample current, 15 minutes) and annealing (350 °C for 15 minutes

followed by a flash to 400 °C for two minutes). The temperature was measured by a chromel–alumel thermocouple in direct contact with the sample. This resulted in a clean surface as determined by HREELS and AES, and a sharp c(8 × 2) LEED pattern which corresponds to an In-terminated surface [18]. HREEL spectra were recorded with low incident electron energies (E_i) ranging from 1.25 to 10 eV and in specular scattering geometry ($\theta_i = \theta_s = 45°$). The resolution of the elastic peak varied significantly (between 3.5 and 7 meV full width at half-maximum) with incident electron energy and sample reflectivity.

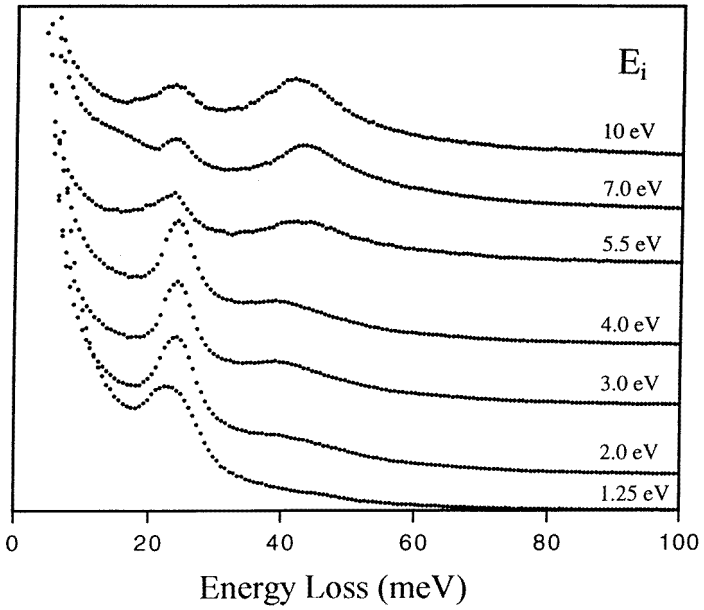

Figure 1. Specular ($\theta_i = \theta_s = 45°$) HREEL spectra, recorded with $E_i = 1.25$–10.00 eV, from an ion-bombarded and annealed n-type (Si-doped, $n \sim 5 \times 10^{17}$ cm^{-3}) InSb(100) surface. All of the spectra are normalized to the specular elastic peak.

3. Results and analysis

The experimental results and general features of our model are introduced first, followed by a discussion of the two-, three- and four-layer models in turn. A series of normalized specular HREEL spectra, taken at various incident electron energies from clean InSb(100), is shown in figure 1. At the lowest electron energy (1.25 eV), a single loss feature is observed at 24 meV. This is the Fuchs–Kliewer surface optical phonon mode [2] and its intensity increases between 1.25 and 2 eV, before decreasing as the electron beam energy is further increased to 10 eV. A second, broader loss feature is also observed at 43 meV. This feature becomes evident at 2 eV and increases in intensity as the electron beam energy is raised to 10 eV. This is assigned to the electron plasmon excitation arising from free carriers within the conduction band. The effective probing depth at 10 eV is approximately 400 Å for the plasmon excitation (and 750 Å for the phonon excitation), so the HREEL spectra are sensitive to the whole space-charge region.

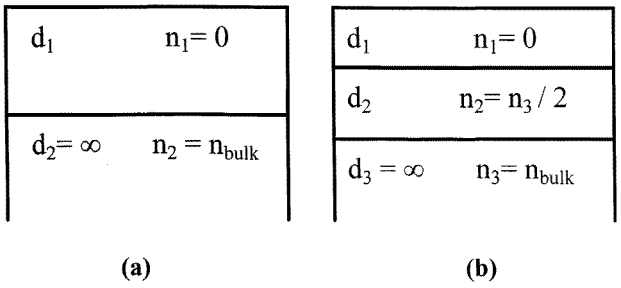

Figure 2. A schematic representation of (a) the two- and (b) the three-layer models used to simulate the experimental HREEL spectra, showing the layer thicknesses and charge densities.

Semi-classical dielectric theory was used to simulate the HREEL spectra [9, 19]. Comparisons were made between two-, three- and four-layer models in describing the charge distribution in the near-surface region of the material (figure 2). The dielectric functions of the layers are given by

$$\varepsilon_i(q,\omega) = \varepsilon(\infty)\left[1 + \frac{\omega_{ph}^2}{\omega_{TO}^2 - \omega^2 - \mathrm{i}\gamma\omega} - \frac{\omega_i^2}{\omega^2 - \beta_i^2 q^2 + \mathrm{i}\omega\Gamma_i}\right] \tag{1}$$

where q and ω are the excitation wavevector and frequency respectively, $\varepsilon(\infty)$ is the high-frequency dielectric constant (15.68 for InSb) [20] and ω_{ph}, γ and ω_{TO} are the phonon strength parameter, damping parameter and frequency respectively. These last three parameters were constant for all of the layers. The final term in equation (1) represents the plasmon response, with the plasma frequencies ω_i being related to the effective mass (m^*) and carrier concentration (n_i) by $\omega_i^2 = n_i e^2/\varepsilon_0\varepsilon(\infty)m^*$. Note that ω_1 is set to zero for all of the calculations.

The two-band Kane model [21] was used to calculate the Fermi level, carrier velocity at the Fermi level, effective mass at the Fermi level, plasma frequency and the Thomas–Fermi screening length. The spatial dispersion parameters (β_i) are described within the Thomas–Fermi model, and for a degenerate electron gas, β is related to the velocity of the electrons at the Fermi level (v_F) by $\beta^2 = (3/5)v_F^2$. Values for the spatial dispersion coefficients were calculated from the Fermi velocities in each layer. The values of the plasmon damping in each layer (Γ_i) were treated as free parameters. Note that the effects on the spectra of the finite acceptance angle of the analyser, although relatively minor, are fully incorporated in the calculations.

3.1. The two-layer model

The two-layer model is illustrated in figure 2(a) and consists of a carrier-free layer on top of the semi-infinite bulk. Simulated HREEL spectra based on the two-layer model are shown in figure 3 along with the corresponding experimental data. For all incidence energies, the simulated curves reproduce the features of the plasmon and phonon peaks extremely well. The best fits were obtained with a bulk plasma frequency (ω_2) of 47 meV, which corresponds to a bulk carrier concentration of 8×10^{17} cm^{-3}, a value slightly higher than the nominal bulk doping level of the sample. The fitting of the spectra proved to be extremely sensitive to the depletion layer thickness (d_1) and the plasmon damping (Γ_2). To reproduce the spectra over the range of incident electron energies studied (1.25–10 eV), values of

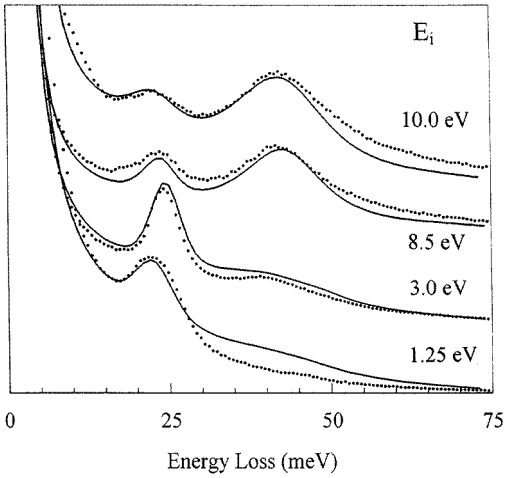

Figure 3. Experimental HREEL spectra (dotted lines) for InSb(100) with $E_i = 1.25$, 3.00, 8.50 and 10.00 eV. Also shown are the best-fit spectra (solid lines) simulated using the two-layer model shown in figure 2(a).

$d_1 = 84$ Å and $\beta_2 = 0.61 \times 10^6$ m s^{-1} were used [22]. It was also necessary to vary Γ_2 with the electron beam energy. The depletion layer thickness was determined solely by the fitting procedure and was not referenced to the charge profile calculations. The abrupt charge profile is able to simulate the HREEL spectra very well (figure 3) despite being only a crude approximation to the true charge distribution, since d_1 is approximately equal to L_{TF}. The spatial dispersion parameter β_2 used for the best-fit simulations is slightly less than that calculated from the Thomas–Fermi model ($\beta_{calc} = 0.75 \times 10^6$ m s^{-1}). Similar values were obtained from recent HREELS studies of heavily doped ($n \sim 7 \times 10^{18}$ cm^{-3}) InSb(100) surfaces prepared by non-grazing-incidence ion bombardment [11]. In that case, the experimentally determined β-value was significantly less than the calculated value (0.43×10^6 m s^{-1} compared with 1.12×10^6 m s^{-1}). We have previously suggested that the high defect density in the near-surface region resulting from the ion bombardment process reduces the spatial dispersion coefficient by increasing the scattering rate of carriers, such that their mean velocity is considerably less than the Fermi velocity [11]. Although a similar effect is evident in this experiment, the reduction is far less significant. This is likely to be due to the grazing-incidence ion bombardment conditions employed here, since we have shown recently that such treatment of InAs(001) results in less residual damage than bombardment at higher angles [23]. We also note that the increase of carrier concentration beyond the bulk doping level due to bombardment-induced defects is much less in this experiment (3×10^{17} cm^{-3} compared with 2×10^{18} cm^{-3} in reference [11]) most probably for the same reason.

The plasmon damping factors obtained from the two-layer model simulations are shown in figure 4 (solid circles) as a function of incident electron energy. The damping decreases with increasing electron beam energy, such that $\Gamma_1 = 167$ meV at $E_i = 1.25$ eV and 91 meV at $E_i = 10$ eV. In a recent HREELS study of InAs(100) surfaces we have also shown that the plasmon damping increases at low electron beam energies [13]. In this study, the damping was modelled using contributions from surface Ohmic damping, bulk Ohmic damping and Landau damping. Surface and Landau damping were found to be dominant

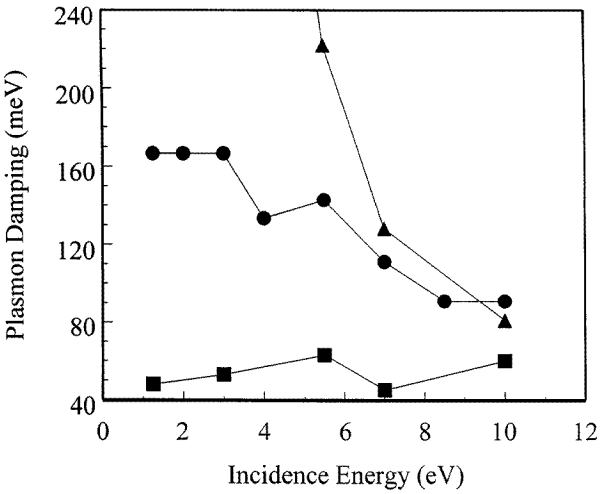

Figure 4. Best-fit values for the bulk plasma damping Γ_2, deduced from the two-layer model (circles), as a function of E_i. Also shown are best-fit values for Γ_3 (triangles) and Γ_4 (squares) deduced from the four-layer model.

at low electron beam energies, as expected from the high plasmon wavevectors and low effective probing depth. The two-layer model would therefore lead us to assume that the increase in plasmon damping at low incidence energies for InSb is also due to surface scattering and Landau damping. However, the two-layer model cannot take into account spatial variation of the plasmon lifetime since there is only one uniform layer which is electronically active. In order to investigate this variation it is necessary to use additional layers in the model.

3.2. The three-layer model

A layer of intermediate carrier concentration (half that of the bulk value) was introduced into the two-layer model as shown in figure 2(b). This modification was made somewhat arbitrarily and the resulting charge profile was not intended to reflect in detail the calculated distribution. The plasmon damping parameter of the intermediate layer (Γ_2) was treated as a free parameter, with fixed layer thicknesses d_1 and d_2. Fits of a similar quality to the two-layer model simulations could be obtained at all incidence energies. The layer thicknesses d_1 and d_2 were fixed at 60 Å and 35 Å respectively, representing some smoothing of the abrupt profile.

Examples of simulated HREEL spectra based on the three-layer model, together with an experimental spectrum recorded at $E_i = 3$ eV, are shown in figure 5. The value of Γ_2 was varied between 167 meV (equal to the bulk damping value for this incidence energy, as deduced from the two-layer model) and 10^4 meV. Surprisingly, a satisfactory fit was only obtained using the highest damping parameter, which represents an extreme and physically unrealistic overdamping of the plasmon. With lower damping values, the intensity of the phonon peak is reduced and there is a significant increase of intensity on both sides of this peak. These intensity changes can be explained by considering the coupling of the plasmon and phonon excitations in the intermediate layer.

Figure 6 shows the surface loss functions which correspond to the simulated HREEL

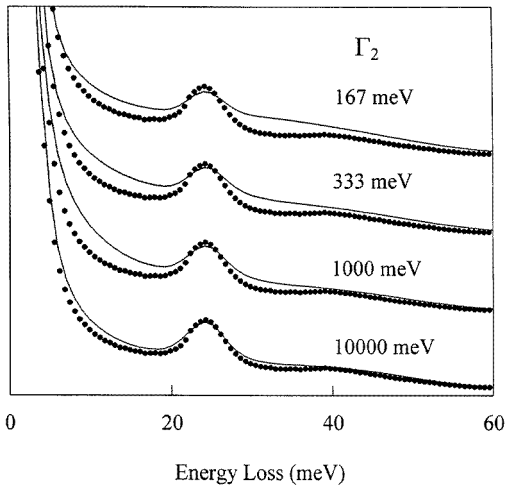

Figure 5. HREEL spectra simulated using the three-layer model (solid lines) at $E_i = 3$ eV, varying the bulk plasma damping Γ_2. Also shown is the corresponding experimental HREEL spectrum (dotted lines).

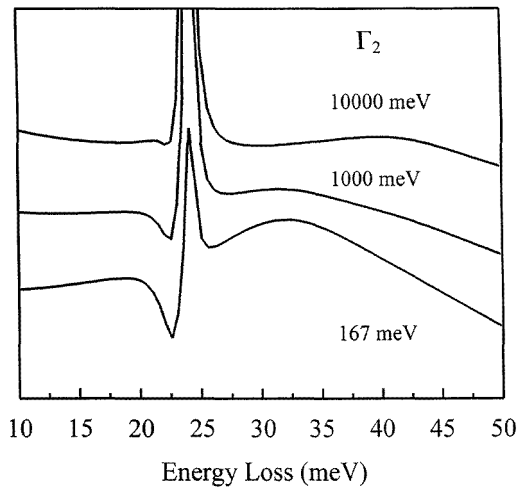

Figure 6. The surface loss functions used in the HREELS simulations shown in figure 5 for an electron beam energy of 3 eV. Note the additional features on both sides of the phonon peak with low plasmon damping Γ_2.

spectra shown in figure 5. With low plasmon damping in the intermediate layer (layer 2), two additional features appear on either side of the phonon peak at loss energies of 19 meV and 32 meV. These features are not present in the spectra calculated with high plasma damping, and are seen only as additional intensity in the full simulated spectra (figure 5) because of the inclusion of the instrumental broadening. They can be assigned to the coupled plasmon–phonon or 'plasmaron' modes in layer 2 [6, 24]. A simple calculation of the coupled-mode dispersion shows that the plasmon and phonon excitations are only resonant in the intermediate layer, not in the bulk. Interfacial plasmon modes are not responsible for the additional intensity since the probing depth at $E_i = 3$ eV is approximately twice the largest layer thickness, so all of the modes are surface-like rather than interface-like [12]. Furthermore, a high bulk plasmon damping would be required to damp out an interface mode propagating between layers 2 and 3, but this is not required since only the damping in layer 2 needs to be increased.

The three-layer model introduces plasmaron modes propagating in layer 2 which are

not observed experimentally and which can only be removed by introducing very high and physically unrealistic plasmon damping. This indicates that the homogeneous intermediate layer provides a poor description of the rapidly varying charge density at the boundary of the depletion region. The high effective damping ('structural' damping) of the plasmon in this region is a real effect that can be thought of as due to the interaction of several very thin plasma layers of similar frequencies. The combination of many allowed wavevectors due to the finite angular resolution of HREEL spectrometers contributes to this effect [25]. A smooth spatial distribution of plasma frequencies indeed produces a higher effective plasma damping in regions of rapid charge-density variation, as observed by Chen *et al* in a comparative study of two-layer and smooth models of the GaAs(110) depletion region [6]. The presence of structural plasmon damping represents a limitation of the HREELS method and local dielectric models in describing regions of rapidly varying plasma frequency, since it may mask more useful information concerning Ohmic and Landau damping. In this case, the abrupt model clearly gives a superior account of the data since the three-layer model must be modified so as to make the intermediate layer electronically inactive.

3.3. The four-layer model and the calculated charge profile

The two- and three-layer models were both constructed without reference to a specific charge profile, through the fitting of the HREEL spectra. However, it is preferable to develop a model based on an independently determined charge profile. The calculation of such a charge profile requires a full self-consistent solution of the Schrödinger and Poisson equations, as applied by Ehlers and Mills [26] to GaAs. Their calculation ignored non-parabolicity of the conduction band, an approximation that is inappropriate for InSb [21]. However, an alternative approach, termed the 'modified Thomas–Fermi approximation' (MTFA), was developed by Zöllner *et al* [27] for inversion layers in InSb, and this can readily be adapted to describe a depletion layer [28]. The MTFA involves the calculation of a classical potential $V(z)$, which is then used to compute $n(z)$ according to the equation

$$n(z) = N_c \frac{2}{\sqrt{\pi}} (k_B T)^{-3/2} \int_0^\infty \frac{\sqrt{E}\sqrt{1 + E/E_g}(1 + 2E/E_g)}{1 + \exp([E - E_F + V(z)]/k_B T)} \, f(z) \, \mathrm{d}E \tag{2}$$

where

$$f(z) = 1 - \sin\left(\frac{2z}{L}\sqrt{\frac{E}{k_B T}}\sqrt{1 + \frac{E}{E_g}}\right) \Big/ \left(\frac{2z}{L}\sqrt{\frac{E}{k_B T}}\sqrt{1 + \frac{E}{E_g}}\right) \tag{3}$$

and

$$L = \frac{\hbar}{2m_0^* k_B T}.$$

In the above equations, E_g is the band gap, E_F is the bulk Fermi level, N_c is the effective density of states in the conduction band (4.3×10^{16} cm^{-3} for InSb at room temperature), m_0^* is the effective mass of the electrons at the conduction band minimum ($0.0136 m_e$) and L is a thermal unit of length (105 Å).

Non-parabolicity is included by using a Kane-type density of states in the Fermi integral over the conduction band [21] and has a very significant effect on the resulting charge profile. The effects of the surface potential barrier are incorporated by the function $f(z)$, which decreases smoothly to zero at the surface ($z = 0$), reflecting the behaviour of the electron wavefunctions in the vicinity of the effectively infinite surface barrier. This has a relatively small effect in the case of a depletion layer since the unmodified classical charge

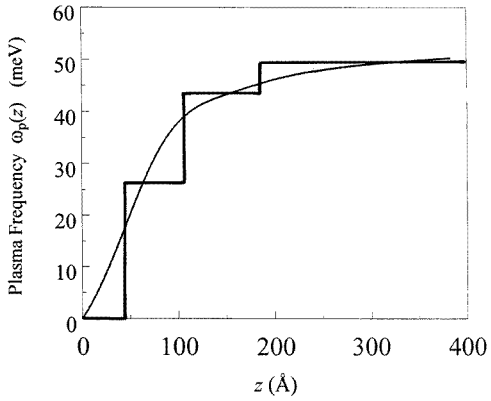

Figure 7. The plasma frequency profile $\omega_p(z)$ for InSb calculated using the MTFA. The four-layer approximation used in HREELS simulations is also shown.

density is very low near the surface. Compared with the full self-consistent approach [26], the computational requirements are relatively modest and the non-parabolicity is accounted for. Numerical solution of the Poisson equation is straightforward, using equation (2) to compute the classical potential (i.e. $V(z)$ with $f(z)$ equal to unity). The classical potential is then used to calculate the carrier concentration and hence the plasma frequency as a function of depth, including $f(z)$ to describe the surface barrier effects. The calculated plasma frequency profile for InSb at room temperature is shown in figure 7. We have assumed a zero ionization energy for the donors, due to screening [29], giving a uniform positive background throughout the space-charge layer. It should also be noted that with the non-parabolicity correction, the plasma frequency levels off more rapidly at large depths (>150 Å) due to the increasing electron effective mass as the Fermi level rises to its bulk value (122 meV above the conduction band minimum). It is evident that the space-charge region extends considerably deeper than the two-layer fitting ($d_1 = 84$ Å) of the HREEL spectra would suggest, but that the non-parabolicity limits the inhomogeneity in plasma frequency at large depths.

Table 1. Parameters for the four-layer simulations. The Γ_i values are deduced from best fits to the HREELS data and vary with E_i, whereas the other parameters are fixed.

Parameter	$i = 1$	$i = 2$	$i = 3$	$i = 4$
d_i (Å)	40	50	90	∞
ω_i (meV)	0	26	44	49
Γ_i (meV) with $E_i = 10$ eV	n/a	10 000	86	59
Γ_i (meV) with $E_i = 3$ eV	n/a	10 000	625	53
β_i (10^6 m s^{-1})	n/a	0.38	0.56	0.62

The calculated charge distribution was approximated by four uniform regions as shown in figure 7. The experimental HREEL spectra were simulated using this four-layer model, with a fixed charge profile. The only free parameters were the plasma damping parameters. By adjusting these parameters in the individual layers it was possible to produce excellent

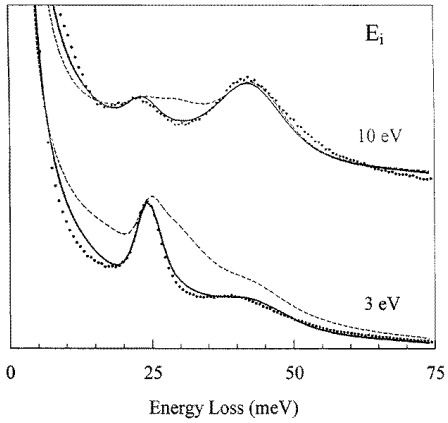

Figure 8. Simulated and experimental (dotted lines) HREEL spectra with $E_i = 3$ eV and 10 eV. The simulated spectra were generated using a four-layer model to approximate the MTFA charge profile. Solid lines indicate best fits, and dashed lines indicate poor fits caused by low plasmon damping (100 meV) in layer 2.

fits to the experimental HREEL spectra using this more realistic profile (shown in figure 8 for $E_i = 3$ eV and 10 eV). The solid lines indicate the best fits, and the dashed lines represent simulated spectra which differ from the best fits only in the parameter Γ_2 (set to 100 meV rather than the overdamping 10^4 meV needed for the best fits). All of the best-fit parameters are summarized in table 1. This represents the first experimental test of the MTFA model in describing the surface space-charge region of a non-parabolic band semiconductor material.

The overall fits are better than those produced by the two-layer model, primarily in the plasma response at low incidence energies. For example, the discrepancy generated by the two-layer fits in the 30–60 meV loss region for $E_i = 1.25$ eV (figure 3) is absent in the four-layer fits. The layer-2 damping parameter had to be set to 10^4 meV in all of the simulations in order to avoid spurious plasmon–phonon coupling similar to that observed in the three-layer model. Setting this parameter to 100 meV results in pronounced deviation from the experimental data which is consistent with the generation of plasmaron modes. At 3 eV, the phonon peak is shifted to higher loss energy with a large increase of intensity around this peak (figure 8, dashed line). At 10 eV the deviation is confined to the region between the plasmon and phonon peaks: due to the increased probing depth at this energy the uncoupled plasmon is still observable.

The values of the damping parameters in layers 3 and 4 are shown in figure 4 (triangles and squares respectively). The bulk damping Γ_4 is almost constant as a function of E_i, in contrast to the bulk damping of the two-layer model. The value of the damping is lower (an average of 54 meV compared with the lowest value of 90 meV for the two-layer model), giving a bulk electron mobility of 2700 $cm^2\ V^{-1}s^{-1}$. Landau damping cannot influence the damping constant of the bulk layer since the excitations produced in this layer have a maximum wavevector determined by the minimum probing depth (180 Å) for scattering in HREELS [10]. This minimum wavelength is well above the screening length of the electron gas (84 Å), below which Landau damping is expected to become strong, and explains why the bulk damping does not vary with incidence energy.

The damping in the third layer, Γ_3, varies markedly with energy, increasing from 86

meV at 10 eV to 2500 meV at 1.25 eV (triangles in figure 4; the entire range is not shown). This rapid increase is much more pronounced than that observed for the bulk damping in the two-layer model, and results in extreme overdamping of the plasmon at the lowest incidence energies. We ascribe this heavy damping to a combination of Landau damping, surface damping and the additional 'structural' damping required as a result of using the step profile approximation. However, it is difficult to make any quantitative estimate of the relative contributions of these damping mechanisms. This represents a severe limitation of the step profile model which may be critical in the analysis of rapidly varying charge profiles for which quantitative information concerning plasmon damping is needed. For an analysis of the InSb(100) depletion layer system, the crude but commonly used two-layer model, clearly does not give a sufficiently detailed picture of the plasmon damping mechanisms, since it implies an energy dependence for the bulk damping which is incorrect according to the four-layer model. However, when structural damping is present, it may swamp the effects of Ohmic and Landau damping. It is clear that the plasmon damping in layer 2, where the charge variation is most pronounced (figure 7), is dominated by structural damping since a value of 10^4 meV is needed at all of the incidence energies. In layer 3 the charge variation is significantly smaller (figure 7), and the structural damping is correspondingly less. It is not possible, however, to distinguish the structural damping from the Landau damping using this model.

From the MTFA calculation we are able to deduce the band bending and surface state density. We find that the surface Fermi level is pinned in the band gap close to the conduction band minimum, to give a total band bending of 140 meV. The largest value for the band bending with which we are able to fit the HREEL spectra satisfactorily is approximately 180 meV. This indicates that the surface Fermi level is pinned at least 120 meV above the valence band maximum. Evans *et al* [12] found the surface Fermi level of decapped InSb(100) to lie at most 100 meV above the valence band maximum, using HREELS and Ne(I) photoemission. However, their analysis of the HREELS data ignored spatial dispersion and was based on a Schottky depletion model. Both of these approximations are inappropriate for degenerate InSb(100), and the surface state density obtained from the analysis of Evans *et al* [12] (2.5×10^{12} cm^{-2}) is somewhat higher than that from our analysis (1.1×10^{12} cm^{-2}), in line with the increased band bending.

4. Conclusions

The limitations of local dielectric theory and step profile models in simulating HREEL spectra of doped semiconductors have been investigated by applying two-, three- and four-layer models to describe the depletion region of an InSb(001) surface. Experimental HREEL spectra were recorded using low electron beam energies to maximize the sensitivity to the non-uniform charge density in the near-surface region. Good agreement between experimental and simulated spectra was achieved by assuming an abrupt charge profile (the two-layer model) and incorporating spatial dispersion and variable plasmon damping. When the charge profile was adjusted to simulate the non-abrupt nature of the depletion region (the three-layer model), good fits to the data were only obtained using physically unrealistic values for the plasmon damping in the intermediate layer. Very strong 'structural' damping was required to remove the plasmon–phonon coupling in this layer. This reflects the limitations of the homogeneous intermediate layer in describing the highly non-uniform electron gas, and explains why the two-layer model has been so successful despite its crude approximation of the charge profile. A four-layer model, closely approximating the calculated charge distribution, provided excellent fits to the experimental data, without any

need to adjust the charge profile parameters. The damping factors in the layers were varied in order to avoid plasmon–phonon coupling in the depletion region and showed different energy dependence in each of the layers. The structural damping required was greater in regions of more rapid charge variation. The bulk damping was found to be independent of incidence energy, a result qualitatively different from that of the two-layer model. This is due to the suppression of Landau damping in the bulk by the limited wavevector transfer to this region. Although multilayered models can describe the spatial dependence of the plasmon damping, 'structural' damping in regions of rapid charge density variation can mask Landau and Ohmic damping mechanisms.

Acknowledgments

Financial support for this work was provided by the Engineering and Physical Sciences Research Council (EPSRC), UK, under Contract No GR/J83543. The provision of EPSRC studentships for GRB and CPAM is also acknowledged.

References

[1] Matz R and Lüth H 1981 *Phys. Rev. Lett.* **46** 500
[2] Ritz A and Lüth H 1984 *Phys. Rev. Lett.* **52** 1242
[3] Gray-Grychowski Z J, Egdell R G, Joyce B A, Stradling R A and Woodbridge K A 1987 *Surf. Sci.* **186** 482
[4] Egdell R G, Evans S D, Stradling R A, Li Y B, Parker S D and Williams R H 1992 *Surf. Sci.* **262** 444
[5] Betti M G, del Pennino U and Mariani C 1989 *Phys. Rev.* B **39** 5887
[6] Chen Y, Nannarone S, Schaefer J, Hermanson J C and Lapeyre G J 1989 *Phys. Rev.* B **39** 7653
[7] Polyakov V, Elbe A and Schäfer J A 1995 *Appl. Phys.* A **60** 567
[8] Dubois L H, Zegarski B R and Persson B N J 1987 *Phys. Rev.* B **35** 9128
[9] Lucas A A, Vigneron J P, Lambin P, Thiry P A, Liehr M, Pireaux J J and Caudano R 1986 *Int. J. Quantum Chem. Symp.* **19** 687
[10] Ibach H and Mills D L 1982 *Electron Energy Loss Spectroscopy and Surface Vibrations* (New York: Academic)
[11] Jones T S, Schweitzer M O, Richardson N V, Bell G R and McConville C F 1995 *Phys. Rev.* B **51** 17 675
[12] Evans S D, Cao L L, Egdell R G, Droopad R, Parker S D and Stradling R A 1990 *Surf. Sci.* **226** 169
[13] Bell G R, McConville C F and Jones T S 1996 *Phys. Rev.* B **54** 2654
[14] Jones T S, Ding M Q, Richardson N V and McConville C F 1990 *Appl. Surf. Sci.* **45** 85
[15] Jones T S, Ding M Q, Richardson N V and McConville C F 1991 *Surf. Sci.* **247** 1
[16] Inaoka T, Newns D M and Egdell R G 1987 *Surf. Sci.* **186** 290
[17] Ibach H 1991 *Electron Energy Loss Spectroscopy: The Technology of High Performance (Springer Series in Optical Sciences 63)* (Berlin: Springer)
[18] McConville C F, Jones T S, Leibsle F M, Driver S M, Noakes T C Q, Schweitzer M O and Richardson N V 1994 *Phys. Rev.* B **50** 14 965
[19] Lambin P, Vigneron J P and Lucas A A 1990 *Comput. Phys. Commun.* **60**
[20] *Landolt–Börnstein New Series* 1982 Group III, vol 17a, ed K-H Hellwege (Berlin: Springer)
[21] Kane E O 1957 *J. Phys. Chem. Solids* **1** 249
[22] Over the entire range of incidence energies used, the best-fit values for d_1 varied in the range 84 ± 6 Å, while β_2 varied in the range $(0.61 \pm 0.02) \times 10^{-6}$ m s^{-1}.
[23] Bell G R, McConville C F and Jones T S 1996 *Appl. Surf. Sci.* **104+5** 17
[24] Yu H and Hermanson J C 1989 *Phys. Rev.* B **40** 11 851
[25] Chen Y, Hermanson J C and Lapeyre G J 1989 *Phys. Rev.* B **39** 12 682
[26] Ehlers D H and Mills D L 1986 *Phys. Rev.* B **34** 3939
[27] Zöllner J-P, Übensee H, Paasch G, Fielder T and Gobsch G 1986 *Phys. Status Solidi* b **134** 837
[28] Übensee H, Paasch G and Zöllner J-P 1988 *Phys. Rev.* B **39** 1955
[29] Schubert E F 1993 *Doping in III–V Semiconductors* (Cambridge: Cambridge University Press)